

Communication

# Slow Light Effect and Tunable Channel in Graphene Grating Plasmonic Waveguide

Yingqiu Zhang, Xing Liu, Qiaohua Wu, Wenfeng Li and Chunlei Li \*

College of Science, Northeast Forestry University, Harbin 150040, China; zyz19970829@126.com (Y.Z.); liuxing.1998@foxmail.com (X.L.); wqh20786@163.com (Q.W.); w1nfun@163.com (W.L.)

\* Correspondence: licl915@163.com

**Abstract:** A graphene plasmon waveguide composed of silicon grating substrate and a silica separator is proposed to generate the slow-light effect. A bias voltage is applied to tune the optical conductivity of graphene. The tunability of the slow-light working channel can be achieved due to the adjustable bias voltage. With an increase in the bias voltage, the working channel exhibited obvious linear blue-shift. The linear correlation coefficient between the working channel and the bias voltage was up to 0.9974. The average value of the normalized delay bandwidth product (NDBP) with different bias voltages was 3.61. In addition, we also studied the tunable group velocity at a specific working channel. Due to the tunability of this miniaturized waveguide structure, it can be used in a variety of applications including optical storage devices, optical buffers and optical switches.

**Keywords:** slow light effect; graphene; surface plasmon polaritons; normalized delay bandwidth product

## 1. Introduction

Slow-light technology can be applied to non-linear optical devices [1,2], integrated interferometers [3], and all-optical information devices such as optical buffers [4], optical storage devices [5], optical switches [6–8], and so on. So far, electromagnetic induced transparency [9–11], coherent population oscillation [12], stimulated Brillouin scattering [13], photonic crystal waveguide [14], coupling resonance transparency technology [15] and plasmonic waveguide [16] have been found to achieve the slow-light effect. Surface plasmon polaritons (SPPs), an electromagnetic wave that propagates at the interface between metal and dielectric, can break through the diffraction limitation of light [17–21]. At present, the various types of plasmonic waveguides are designed to realize the slow-light effect [16,22,23]. For example, Chen et al. proposed a circular split-ring resonance cavity and a double symmetric rectangular stub waveguide which can produce a maximum optical delay of about 0.128 ps [18]. It can be seen that when the SPPs propagates in the noble metal material waveguides, the slow-light working channel of SPPs propagation is difficult to adjust, which limits their potential for some specific applications.

Graphene has been proposed as a key solution to overcome this problem, as it has unique features in optics, materials, chemistry and so on. Graphene is a single layer of carbon atoms densely arranged in a honeycomb shape, which can replace metal to form SPPs waveguide in the mid-infrared frequency range. Compared with traditional metal materials, graphene has the remarkable characteristics of dynamically tunable conductivity, the broader response spectrum, the higher field confinement, and the lower intrinsic losses [10,24]. In recent years, the field of slow light in the graphene structure has attracted extensive attentions in the research community [8,10,25–31]. For example, Banxian Ruan et al. proposed a metal grating-coupled graphene metamaterial, for which the group delay can be effectively modulated by the grating period and groove, for which the maximum group delay is 0.4 ps [10]. Ran Hao et al. studied the slow-light performances and the large delay-bandwidth product in a graphene-grating waveguide [25]. Lu Hua et al. realized slow light at the edge of the stopband and introduced graded grating to broaden the



**Citation:** Zhang, Y.; Liu, X.; Wu, Q.; Li, W.; Li, C. Slow Light Effect and Tunable Channel in Graphene Grating Plasmonic Waveguide. *Photonics* **2022**, *9*, 54. <https://doi.org/10.3390/photonics9020054>

Received: 15 December 2021

Accepted: 17 January 2022

Published: 20 January 2022

**Publisher's Note:** MDPI stays neutral with regard to jurisdictional claims in published maps and institutional affiliations.



**Copyright:** © 2022 by the authors. Licensee MDPI, Basel, Switzerland. This article is an open access article distributed under the terms and conditions of the Creative Commons Attribution (CC BY) license (<https://creativecommons.org/licenses/by/4.0/>).

spectral region [31]. Although many structures have good slow-light performances, the tunable slow light working channel is rarely discussed. Moreover, convenient adjustment to the working channel will be beneficial to the developments of tunable plasmonic device and optical communication.

In this paper, a waveguide consisting of a single layer of graphene and a silicon grating containing a defect cavity is proposed. First, the Bragg equation is used to set the grating waveguide parameters at a specific frequency (35 THz), and the slow light working channel is formed near the frequency. Next, the influence of the bias voltage on the tunable slow light working channel is discussed. The slow-light performances of the waveguide are comprehensively evaluated by the normalized delay bandwidth product (NDBP). Furthermore, the tunable group velocity at a specific working channel is also studied.

### 2. Structure and Theory

A three-dimensional schematic diagram of the proposed graphene waveguide is shown in Figure 1. The waveguide is composed of single-layer graphene and a silicon grating substrate, between which a silica layer is embedded. The groove period of the grating structure is the sum of  $W_A$  and  $W_B$ . The length and depth of the deep groove are  $W_A$  and  $h_1$ , while the length and depth of the shallow groove are  $W_B$  and  $h_2$ , respectively. The defect cavity whose width is  $W_C$  and depth is  $h_1$ . On each side of the defect, period number is 4 and the defect is located at the ninth site. In addition, a bias voltage is applied to control the conductivity of graphene.

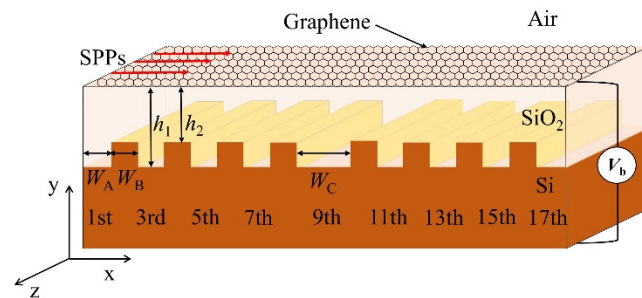


**Figure 1.** Three-dimensional schematic diagram of the proposed graphene waveguide.

At the mid-infrared frequency range, the conductivity of graphene can be simplified into Drude-like equation [30]:

$$\sigma_g = \frac{ie^2\mu_c}{\pi\hbar^2(\omega + i\tau^{-1})} \tag{1}$$

where  $e$  is the electron charge,  $\hbar$  is the reduced plank constant,  $\omega$  is the photon frequency,  $\mu_c$  is the chemical potential and  $\tau$  is the relaxation time. The relaxation time  $\tau$  can be described as  $\tau = \mu\mu_c/(ev_F^2)$ , where  $\mu = 20,000 \text{ cm}^2\text{V}^{-1}\text{s}^{-1}$  is the carrier mobility in graphene and  $v_F = 10^6 \text{ m/s}$  is the Fermi velocity. The chemical potential is defined as  $\mu_c = \hbar v_F(\pi n_s)^{1/2}$ . The doping density  $n_s$  in graphene can be written as  $n_s = \epsilon_d\epsilon_0 V_b/eh$ , here  $\epsilon_d = 3.9$  is the relative permittivity of silica,  $\epsilon_0$  is the dielectric permittivity of the vacuum,  $V_b$  is the bias voltage and  $h$  is the thickness of silica spacer.

For the silica spacer with a thickness of more than 100 nm, the effect of the silicon substrate on the dispersion of SPPs modes can be ignored [31]. Consequently, only the influence of dielectric layers (air and silica) near the graphene is considered in the dispersion relationship. The dispersion relationship of the TM polarization plasmon mode is [27]:

$$\frac{\epsilon_a\epsilon_0}{\sqrt{n_{\text{eff}}^2 - \epsilon_a}} + \frac{\epsilon_d\epsilon_0}{\sqrt{n_{\text{eff}}^2 - \epsilon_d}} = -\frac{ik_0\sigma_g}{\omega} \tag{2}$$

where  $\epsilon_a = 1$  is the relative permittivity of air,  $k_0$  is the wave vector of light in the vacuum. According to Equations (1) and (2), the effective refractive index  $n_{\text{eff}}$  is related to the surface conductivity of graphene, which is determined by the bias voltage  $V_b$  and thickness  $h$ . Figure 2a,b show the  $n_{\text{eff}}$  for different  $h$  and  $V_b$ , respectively. With the bias voltage of 60 V, the deeper thickness  $h$  is, the larger value of the real part of  $n_{\text{eff}}$  will be. Additionally, the real part of  $n_{\text{eff}}$  decreases with the applied bias voltage increasing from 50 V to 70 V while the thickness is 250 nm. Moreover, at the frequency of 35 THz, the value of effective refractive index  $n_{\text{effA}}$  and bias voltage  $V_b$  are linearly and inversely correlated (show in the inset of Figure 2b). Here, the deep groove depth  $h_1$  is set as 250 nm and the shallow groove depth  $h_2$  is set as 100 nm. With the bias voltage of 60 V, the effective refractive index of SPPs in the deep groove and shallow groove are  $n_{\text{effA}} = 91.76 - 0.78i$  and  $n_{\text{effB}} = 58.03 - 0.31i$ , respectively.

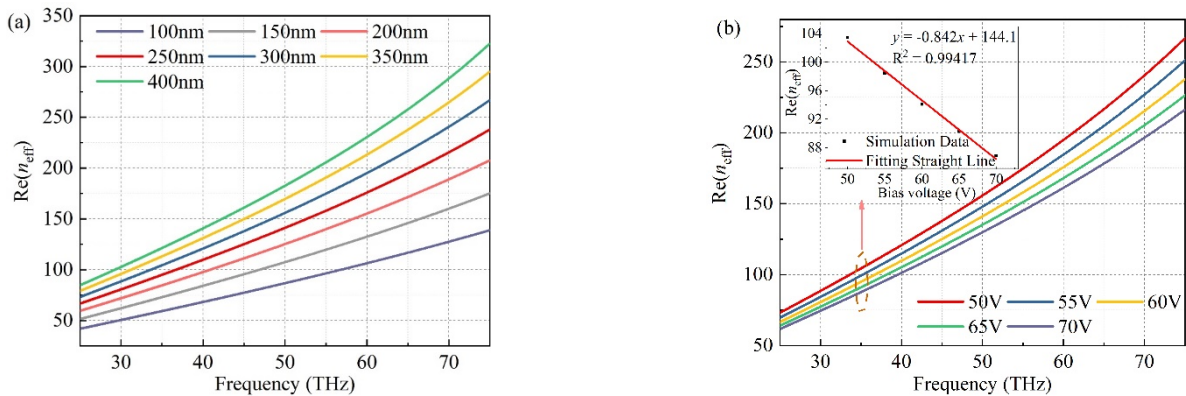


**Figure 2.** Effective refractive index of TM mode at air-graphene-silica structure for different silica layer thicknesses  $h$  with the bias voltage of 60 V (a) and for different gate voltages  $V_b$  with the silica thickness of 250 nm (b). The insets shows that the linear relationship between the effective refractive index and bias voltage at 35 THz.

Corresponding to the central frequency of the stopband, the Bragg scattering condition can be expressed as [32]:

$$W_A \operatorname{Re}(n_{\text{effA}}) + W_B \operatorname{Re}(n_{\text{effB}}) = (2m + 1) \lambda_0 / 2 \tag{3}$$

where  $m$  is an integer assumed to be 0. According to Equation (3),  $\lambda_0$  is the Bragg wavelength, which can be determined by choosing the appropriate groove width  $W$  and effective refractive index  $n_{\text{eff}}$ . In order to make the Bragg wavelength  $\lambda_0 = 8571.4$  nm (center frequency of 35 THz), the widths of the shallow groove and the deep groove of the waveguide are  $W_A = \lambda_0 / 4n_{\text{effA}}$  ( $\sim 23$  nm) and  $W_B = \lambda_0 / 4n_{\text{effB}}$  ( $\sim 37$  nm), respectively. The length of the defect cavity is set as  $W_C = 2W_A$  ( $\sim 47$  nm). Therefore, the total length of the proposed waveguide is 529 nm, which is 3 times smaller than that in Ref. [31]. Thus, the waveguide is more conducive to an improvement of the integration.

### 3. Simulation Results and Discussion

Here, we focus on the slow-light effect in the proposed waveguide. The two-dimensional finite-difference time-domain (2D-FDTD) method (Lumerical FDTD Solutions) with the perfectly matched layer (PML) as the boundary condition is utilized in following calculations. In the FDTD algorithm, the mesh size is no greater than one tenth of the smallest geometric parameter in  $x$  and  $y$  directions to ensure the speed and the accuracy of the simulation. Therefore, the spatial steps are  $\Delta x = 2$  nm,  $\Delta y = 0.1$  nm, which is sufficient for the convergence of numerical results.

Under the bias the voltage is 60 V, the transmission spectrum is calculated, and the result is shown in Figure 3a. A transmission peak with the frequency of 34.77 THz appears

in the stopband. To further explain the generation of the transmission peak, Figure 3b–d shows the electric-field patterns of the incident waves propagating through the Bragg grating and the defect cavity. Figure 3b,d show that the incident waves are reflected at the wavelength of 9084 nm (33 THz) and 8213 nm (36.5 THz), which is in the stopband (shown in Figure 3a). Due to a defect cavity added into the Bragg grating, a defect mode will be produced. When an incident wave propagates in this defect mode, a transmission peak can be formed in the stopband [27]. As displayed in Figure 3c, the incident wave at the wavelength of the transmission peak of 8628 nm (34.7 THz) experienced a strong resonance in the defect cavity and transmits through the structure. The transmission peak means that the waveguide generates the strong normal dispersion effect, which is determined by the Kramers-Kronig relation [33]. The group velocity of SPPs propagation was obtained from the slope of the tangent of a dispersion curve. The dispersion and group velocity of the waveguide are shown in Figure 4a,b, respectively. Obviously, a slow light channel appears in the flat region of dispersion. For frequency of 34.77 THz, a slow light working channel is formed and the minimum value of group velocity is  $0.0028c$  ( $c$  is the light velocity in the vacuum).

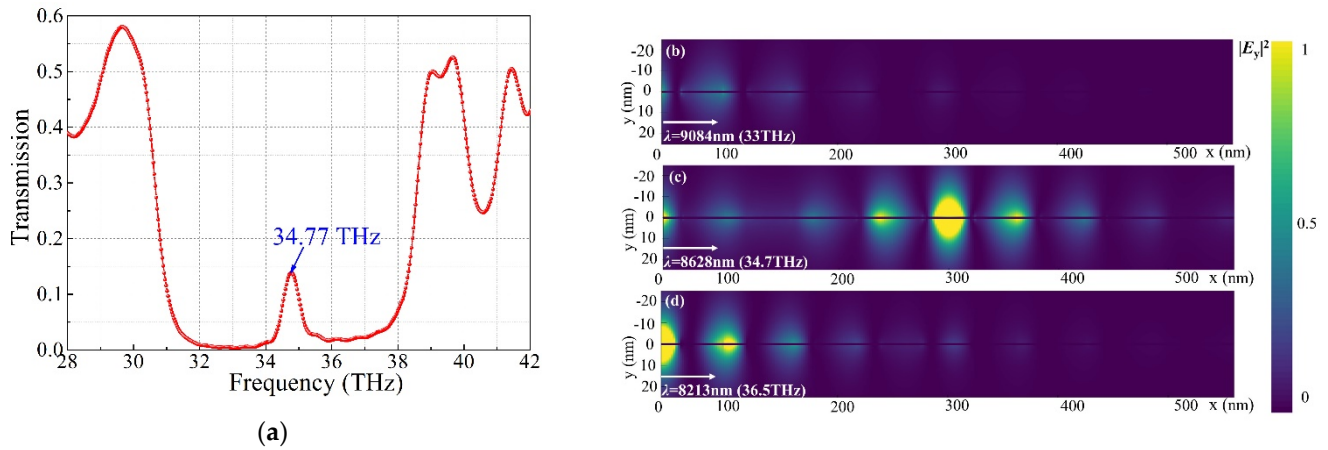


**Figure 3.** (a) Transmission spectrum of the graphene waveguide with bias voltage 60 V. The normalized electric-field patterns from the FDTD simulation for different incident wavelengths: (b) 9084 nm, (c) 8628 nm and (d) 8213 nm.

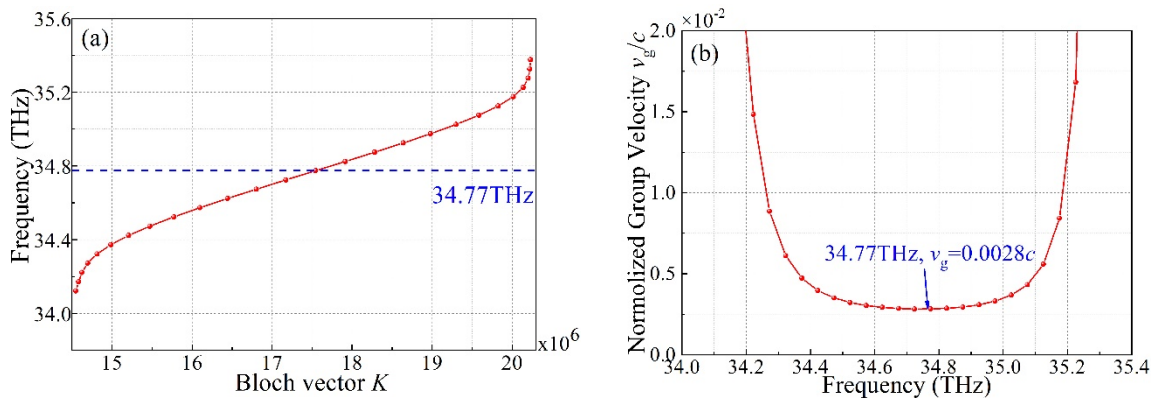


**Figure 4.** (a) Dispersion relationship of the graphene waveguide with bias voltage 60 V. (b) The normalized group velocity  $v_g/c$  of SPPs propagating on interface of graphene waveguide with bias voltage 60 V.

In practice, the fabrication process is extremely complicated, which may lead to the rough surface and small dimensional changes of the waveguide. When the surface of silica is rough, the silica thickness  $h$  is varied, which impacts the chemical potential of

graphene. Therefore, both the roughing surface and small dimensional changes of the waveguide will lead to the variation of dispersion and group velocity. Here, we just focus on the simulation calculation of the group velocity. Thus, we ignored the small changes of structural parameters and suppose that the surface is smooth.

Here, the tunable slow-light working channel is discussed. As seen in Equations (1) and (2), the varying bias voltages result in the changing of the effective refractive index of waveguide, which can tune the frequency of the transmission peak in a fixed structure. From Figure 5a, we can analyze the transmission spectra of the graphene waveguide with different bias voltages. The bias voltage is ranged from 50 V to 70 V with a step of 5 V and the other parameters are set as above. The inset shows that with an increase in the bias voltage, the transmission peak experienced an obvious blue-shift. It indicates that the slow-light working channel has dynamic adjustability.

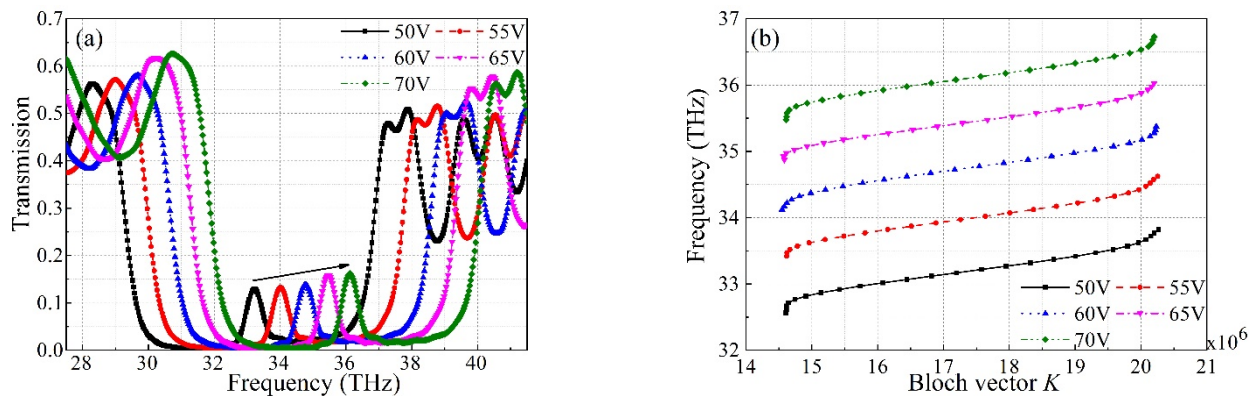


**Figure 5.** (a) Transmission spectra and (b) dispersion relationships of the graphene waveguide with different bias voltages.

Next, the relationship between the group velocity and frequency is shown in Figure 6a. The group velocity of SPPs propagating in each channel shows a considerable decrease. Under the bias voltage from 50 V to 70 V, the minimum group velocity of each channel is approximately equal to  $0.0028c$ . It exhibits that the waveguide has the capability to substantially slow down the propagating speed of SPPs. It clearly shows that the value of the center frequency of the working channel increased linearly with the increase in the bias voltage.

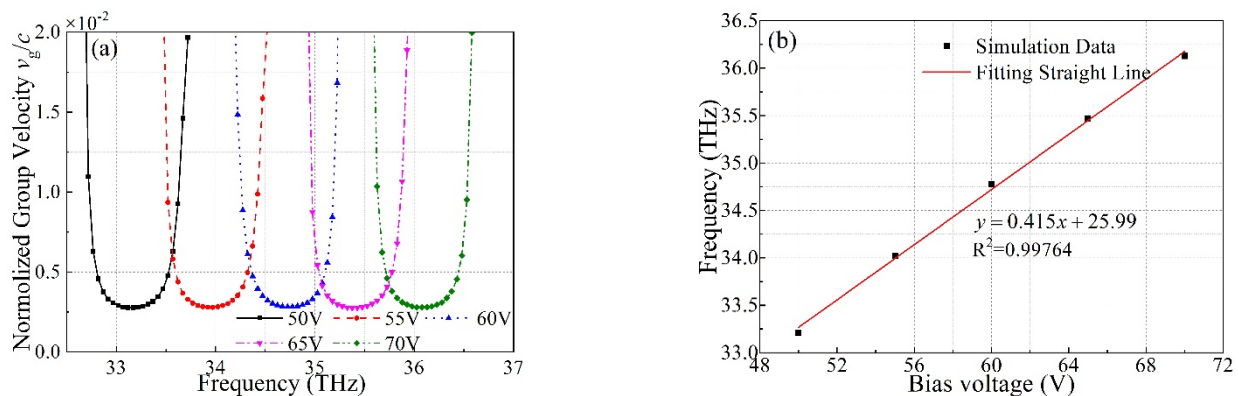


**Figure 6.** (a) The normalized group velocity  $v_g/c$  and (b) center frequencies of the working channel of the graphene waveguide with different bias voltages.

To intuitively observe the linear blue-shift relationship between the center frequency of each slow-light working channel and the different bias voltages, the fitting straight line is revealed in Figure 6b. The linear correlation coefficient is up to 0.9974, which displays a

good linearity. The reason for the linear relationship is that  $\lambda_0$  is inversely proportional to  $n_{\text{eff}}$  and the value of  $n_{\text{eff}}$  increases linearly with the decrease in the bias voltage  $V_b$  (shown in the inset of Figure 2b). When the bias voltage increases from 50 V to 70 V with a step of 5 V, the center frequency of the working channel moves from 33.21 THz to 36.13 THz. The varied range is 2.92 THz.

In addition, to comprehensively evaluate the slow-light performance of the waveguide, the Normalized Delay Bandwidth Product (NDBP) of those channels was calculated. The NDBP was affected by both slowdown factor  $S (= n_g = c/v_g)$  and the bandwidth. We know that  $\text{NDBP} = \tilde{n}_g(\Delta f/f_0)$  [25]. The  $\tilde{n}_g$  is assumed to be constant within  $\pm 10\%$  variation of average value of group index  $n_g$  and the  $\Delta f/f_0$  is the normalized bandwidth. With bias voltage  $V_b$  are 50 V, 55 V, 60 V, 65 V and 70 V, the values of NDBP are 3.70, 3.58, 3.46, 3.48 and 3.83, respectively. Those are all 2.4 times larger than the results of Ref. [25]. In the process of dynamically tuning the channels, each channel has a high NDBP. As a result, the proposed graphene waveguide has the characteristic of a tunable slow-light working channel with good performance.

This proposed waveguide can not only adjust the working frequency of the channel, but also realizes the tunable group velocity for a specific working channel. The group velocity can be reflected by the Gaussian pulse transmission time in the waveguide. We used the working channel with a center frequency of 34.7 THz as an example. Exploiting the FDTD numerical simulation, the normalized transverse magnetic field intensity ( $|H_z|^2$ ) of the SPPs pulse can be observed by the time monitor, the point of which is placed 529 nm away from the source. The input pulse is a TM-polarized Gaussian modulation pulse with a width of 350 fs (full width at half high). Figure 7 shows that the delay time changed with the varying bias voltages. The group velocity is the speed of pulse envelope, which is estimated by the time of pulse propagating through the waveguide. The delay times with bias voltages of 60 V, 65 V and 70 V are 139 fs, 268 fs and 337 fs, respectively. Additionally, the corresponding group velocities are  $0.0127c$ ,  $0.0066c$  and  $0.0052c$ . With the increase in the bias voltages from 60 V to 70 V with a step of 5 V, the varied range of the group velocity is  $0.0074c$ , which reveals that the group velocity can be tunable by altering the bias voltages. As a kind of the tunable slow-speed optical device, the proposed waveguide has great potential in all optical networks.

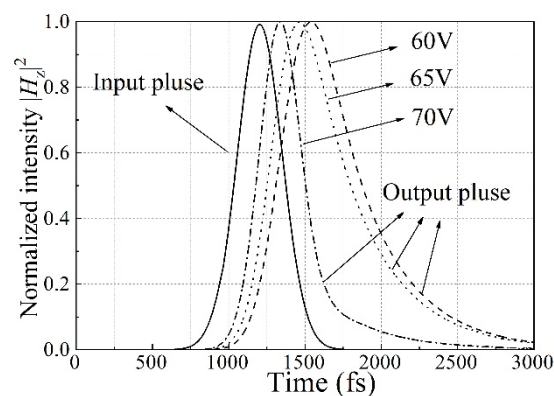


**Figure 7.** The normalized input pulse and output pulse; the input pulse is denoted by the black solid line, and other lines are the output pulse.

#### 4. Conclusions

In conclusion, a graphene Bragg grating waveguide containing a defect was proposed to realize the dynamically tunable slow-light working channel. The waveguide parameters were set using the Bragg equation to ensure the slow-light channel functioned in the 35 THz frequency, with a bias voltage of 60 V. The channel can be tuned by changing the bias voltage. As bias voltage increased, the working channel experienced a linear blue shift. The linear correlation coefficient between the working channel and the bias

voltage was found to be up to 0.9974. Additionally, the waveguide also exhibited a good slow-light performance. The average value of NDBP of each channel is 3.61. Furthermore, the waveguide can also realize the tunable group velocity for a specific working channel. For a pulse with a center frequency of 34.7 THz and width of 350 fs, with the bias voltage varying from 60 V to 70 V, the group velocity changed to 0.0074c. The proposed waveguide has potential applications in tunable plasmonic devices, and optical communication.

**Author Contributions:** The first author Y.Z. has simulated the structure and written the manuscript. The second author X.L. participated in the preparation of the manuscript. The third author Q.W. and the fourth author W.L. gave their opinions on the compilation of the manuscript. Corresponding author C.L. guided the entire work. All authors have read and agreed to the published version of the manuscript.

**Funding:** The Fundamental Research Funds for the Central Universities of China, grant number 2572021DJ05.

**Institutional Review Board Statement:** Not applicable.

**Informed Consent Statement:** Not applicable.

**Data Availability Statement:** The data presented in this study are available on request from the corresponding author.

**Conflicts of Interest:** The authors declare no conflict of interest.

## References

1. Li, P.; Dolado, I.; Alfaro-Mozaz, F.J.; Casanova, F.; Hueso, L.E.; Liu, S.; Edgar, J.H.; Nikitin, A.Y.; Vélez, S.; Hillenbrand, R. Infrared hyperbolic metasurface based on nano structured van der Waals materials. *Science* **2018**, *359*, 892–896. [[CrossRef](#)]
2. Wang, R.Z.; Cao, T. Reconfigurable slow light in phase change photonic crystal waveguide. *J. Appl. Phys.* **2020**, *128*, 163104. [[CrossRef](#)]
3. Torrijos-Morán, L.; Griol, A.; Garcia-Ruperez, J. Slow light bimodal interferometry in one-dimensional photonic crystal waveguides. *Light Sci. Appl.* **2021**, *10*, 1–12. [[CrossRef](#)]
4. Keshavarz, A.; Zakery, A. A Novel Terahertz Semiconductor Metamaterial for Slow Light Device and Dual-Band Modulator Applications. *Plasmonics* **2017**, *13*, 459–466. [[CrossRef](#)]
5. Deng, H.G.; Tian, L.L.; Xiong, R.J.; Liu, G.; Yang, K.; Zhao, H.H.; Wang, W.H. Review on plasmon induced transparency based on metal-dielectric-metal waveguides. *J. Cent. South Univ.* **2020**, *27*, 698–710. [[CrossRef](#)]
6. Khani, S.; Danaie, M.; Rezaei, P. Hybrid All-Optical Infrared Metal-Insulator-Metal Plasmonic Switch Incorporating Photonic Crystal Bandgap Structures. *Nanostructures-Fundam. Appl.* **2020**, *40*, 100802. [[CrossRef](#)]
7. Cai, W.; Xiao, B.; Yu, J.; Xiao, L.H. A compact graphene metamaterial based on electromagnetically induced transparency effect. *Opt. Commun.* **2020**, *475*, 126266. [[CrossRef](#)]
8. Liu, Z.; Gao, E.; Zhang, Z.B.; Li, H.J.; Xu, H.; Zhang, X.; Luo, X.; Zhou, F.Q. Dual-Mode On-to-Off Modulation of Plasmon-Induced Transparency and Coupling Effect in Patterned Graphene-Based Terahertz Metasurface. *Nanoscale Res. Lett.* **2020**, *15*, 1–9. [[CrossRef](#)]
9. Wang, B.Y.; Zhu, Y.H.; Zhang, J.; Zeng, Q.D.; Du, J.; Wang, T.; Yu, H.Q. An ultrafast and low-power slow light tuning mechanism for compact aperture-coupled disk resonators. *Chinese Phys. B* **2020**, *29*, 377–386. [[CrossRef](#)]
10. Ruan, B.; Xiong, C.; Liu, C.; Li, M.; Wu, K.; Li, H. Tunable plasmon-induced transparency and slow light in a metamaterial with graphene—ScienceDirect. *Results Phys.* **2020**, *19*, 103382. [[CrossRef](#)]
11. Islam, M.; Dhriti, K.M.; Sarkar, R.; Kumar, G. Tunable control of electromagnetically induced transparency effect in a double slot terahertz waveguide. *Opt. Commun.* **2020**, *483*, 126632. [[CrossRef](#)]
12. Bigelow, M.S.; Lepeshkin, N.N.; Boyd, R.W. Superluminal and slow light propagation in a room-temperature solid. *Science* **2003**, *301*, 200–202. [[CrossRef](#)] [[PubMed](#)]
13. Schneider, T. Time delay limits of stimulated-Brillouin-scattering-based slow light systems. *Opt. Lett.* **2007**, *31*, 1398–1400. [[CrossRef](#)] [[PubMed](#)]
14. Rawal, S.; Sinha, R.K.; De La Rue, R.M. Slow light miniature devices with ultra-flattened dispersion in silicon-on-insulator photonic crystal. *Opt. Express* **2009**, *17*, 13315–13325. [[CrossRef](#)] [[PubMed](#)]
15. Wang, G.X. Slow light engineering in periodic-stub-assisted plasmonic waveguide. *Appl. Opt.* **2013**, *52*, 1799–1804. [[CrossRef](#)]
16. Chen, J.F.; Li, J.N.; Liu, X.; Rohimah, S.; Tian, H.; Qi, D.W. Fano resonance in a MIM waveguide with double symmetric rectangular stubs and its sensing characteristics. *Opt. Commun.* **2020**, *482*, 126563. [[CrossRef](#)]
17. Liu, X.; Li, J.N.; Chen, J.F.; Rohimah, S.; Li, J.F. Fano Resonance Based on D-shaped Waveguide Structure and Its Application for Human Hemoglobin Detection. *Appl. Optics.* **2020**, *59*, 6424–6430. [[CrossRef](#)]

18. Christensen, J.; Manjavacas, A.; Thongrattanasiri, S.; Koppens, F.H.L.; García de Abajo, F.J. Graphene plasmon waveguiding and hybridization in individual and paired nanoribbons. *ACS Nano* **2012**, *6*, 431–440. [[CrossRef](#)] [[PubMed](#)]
19. Kim, J.T.; Choi, S.Y. Graphene-based plasmonic waveguides for photonic integrated circuits. *Opt. Express* **2011**, *19*, 24557–24562. [[CrossRef](#)]
20. Li, J.N.; Chen, J.F.; Liu, X.; Tian, H.; Wang, J.F.; Cui, J.G.; Rohimah, S. Optical sensing based on multimode Fano resonances in MIM waveguide system with X-shaped resonant cavities. *Appl. Opt.* **2021**, *60*, 5312–5319. [[CrossRef](#)] [[PubMed](#)]
21. Liu, X.; Li, J.N.; Chen, J.F.; Rohimah, S.; Tian, H.; Wang, J.F. Independently tunable triple Fano resonances based on MIM waveguide structure with a semi-ring cavity and its sensing characteristics. *Opt. Express* **2021**, *29*, 20829–20838. [[CrossRef](#)] [[PubMed](#)]
22. Grigorenko, A.; Polini, M.; Novoselov, K. Graphene plasmonics. *Nat. Photon.* **2012**, *6*, 749–758. [[CrossRef](#)]
23. Xia, S.X.; Zhai, X.; Huang, Y.; Liu, J.Q.; Wang, L.L.; Wen, S.C. Graphene Surface Plasmons with Dielectric Metasurfaces. *J. Lightwave Technol.* **2017**, *35*, 4553–4558. [[CrossRef](#)]
24. Xia, S.X.; Zhai, X.; Huang, Y.; Liu, J.Q.; Wang, L.L.; Wen, S.C. Multi-band perfect plasmonic absorptions using rectangular graphene gratings. *Opt. Lett.* **2017**, *42*, 3052–3055. [[CrossRef](#)]
25. Hao, R.; Peng, X.L.; Li, E.P.; Xu, Y.; Jin, J.M.; Zhang, X.M.; Chen, H.S. Improved Slow Light Capacity in Graphene-based Waveguide. *Sci. Rep.* **2015**, *5*, 15335. [[CrossRef](#)]
26. Ghaderian, P.; Habibzadeh-Sharif, A. Rainbow trapping and releasing in graded grating graphene plasmonic waveguides. *Opt. Express* **2021**, *29*, 3996–4009. [[CrossRef](#)]
27. Mao, D.; Cheng, C.; Wang, F.F.; Xiao, Y.H.; Li, T.T.; Chang, L.; Soman, A.; Kananen, T.; Zhang, X.; Kraiank, M.; et al. Device architectures for low voltage and ultrafast graphene integrated phase modulators. *IEEE J. Sel. Top. Quantum Electron.* **2021**, *27*, 1–9. [[CrossRef](#)] [[PubMed](#)]
28. Xia, S.X.; Zhai, X.; Wang, L.L.; Wen, S.C. Plasmonically induced transparency in double-layered graphene nanoribbons. *Photonics Res.* **2018**, *6*, 692–702. [[CrossRef](#)]
29. Xia, S.X.; Zhai, X.; Wang, L.L.; Wen, S.C. Plasmonically induced transparency in in-plane isotropic and anisotropic 2D materials. *Opt. Express* **2020**, *28*, 7980–8022. [[CrossRef](#)]
30. Hanson, G.W. Quasi-transverse electromagnetic modes supported by a graphene parallel-plate waveguide. *J. Appl. Phys.* **2008**, *104*, 084314. [[CrossRef](#)]
31. Lu, H.; Zeng, C.; Zhang, Q.M.; Liu, X.M.; Hossain, M.M.; Reineck, P.; Gu, M. Graphene-based active slow surface plasmon polaritons. *Sci. Rep.* **2015**, *5*, 8443. [[CrossRef](#)] [[PubMed](#)]
32. Hossieni, A.; Massoud, Y. A low-loss metal-insulator-metal plasmonic bragg reflector. *Opt. Express* **2006**, *14*, 11318–11323. [[CrossRef](#)] [[PubMed](#)]
33. Kador, L. Kramers-Kronig relations in nonlinear optics. *Appl. Phys. Lett.* **1995**, *66*, 2938. [[CrossRef](#)]